ANALYTICAL STUDY ON ELASTO-PLASTIC SEISMIC BEHAVIOR OF CIRCULAR STEEL BRIDGE PIER RETROFITTED BY EXTERNALLY BONDED CARBON FIBER SHEETS

Kim Oliver U. MAGTAGÑOB[1], Visal THAY[2], Hitoshi NAKAMURA[3] and Takahiro MATSUI[4]

[1]Master's Course Student, Graduate School of Urban Environmental Sciences, Tokyo Metropolitan University
(1-1 Minami-Osawa, Hachioji, Tokyo 192-0397, Japan)
E-mail: magtagnob-kim-oliver-untalan@ed.tmu.ac.jp
[2]Member of JSCE, Post Doctoral Fellow, Graduate School of Urban Environmental Sciences, Tokyo Metropolitan University
(1-1 Minami-Osawa, Hachioji, Tokyo 192-0397, Japan)
E-mail: visal-thay@tmu.ac.jp
[3]Member of JSCE, Associate Professor, Graduate School of Urban Environmental Sciences, Tokyo Metropolitan University
(1-1 Minami-Osawa, Hachioji, Tokyo 192-0397, Japan)
E-mail: hnaka@tmu.ac.jp
[4]First Advanced Composites Technical Department, Toray Industries, Inc.
(2-1-1 Nihonbashi Muromachi, Chuo-ku, Tokyo , Japan)
E-mail: Takahiro_Matsui@nts.toray.co.jp

In this study, the retrofitting effect of carbon fiber (CF) sheet wrapping method on circular steel piers subjected to cyclic loading was evaluated quantitatively using finite element analysis. To verify the accuracy of the finite element analysis model, the analytical results were compared with the experimental results obtained from the previous study. The circular steel specimen was subjected to an axial force equivalent to 10% of yield axial force and a gradually increasing cyclic transverse load at the top of the specimen. Two retrofitting method were considered, first is the wrapping of seven layers of CF sheet before the loading of the specimen (reinforced specimen) and the latter is the wrapping of CF sheets after the specimen has undergone ultimate failure (repaired specimen). For the finite element analysis model, the column specimen was modeled as 4-node shell elements while CF sheet was modeled as 2-node truss elements. The validity of the analysis model was verified by considering the appropriate constitutive law for the steel specimen and by investigating the mode of application of the vertical loading. For the CF sheet elements, the capacity to resist compressive forces and presence of initial stresses were considered. The results showed that the reinforcement model can quantitatively evaluate the horizontal loading capacity and the buckling mode. For the repaired model, the horizontal loading capacity can be approximately evaluated as well, but is limited to the range where the horizontal displacement is small.

Key Words : *carbon fiber sheet, circular steel bridge pier, seismic retrofitting, buckling, finite element analysis*

1. INTRODUCTION

In Japan, the number of structures reaching 50 years and older will double from its current number in the next two decades. With the ever-increasing number of aging infrastructures, the need to repair and maintain these structures are becoming imperative. In particular, circular steel piers are prone to locally buckle during an occurrence of a strong earthquake[1)]. Being commonly used in urban areas, damage to this structure can have a huge impact after an event of a strong earthquake. Thus, an efficient seismic retrofitting method is needed for the emergency

restoration of buckled steel piers. As a general seismic retrofitting method for existing steel piers, concrete filling method and steel jacketing have been adopted. However, heavy machinery and long construction period are needed for construction, and they do not have good workability and efficiency considering the working space and weight increase.

To address this issue, the application of carbon fiber (CF) sheet winding method is being promoted[2), 3)]. CF sheets are lightweight, high-strength, durable materials that are easy to install. This material is widely used as one of the seismic reinforcement applications for concrete structures. However, it is hardly applied to steel structures.

Experimental studies have been conducted on CF sheet wrapping reinforcement[4) - 6)] for circular steel piers, and local buckling can be reduced by wrapping multiple layers of CF sheet in the circumferential direction. It has been stated that the occurrence of plastic deformation can be slowed by suppressing the occurrence which results to improved toughness. Thus, it has been proposed as a method of seismic retrofitting for steel piers[3)].

In addition, an experimental study on performance recovery when a CF sheet is externally bonded on a circular steel bridge pier that has been buckled has been conducted[7)]. It has been clear that buckling has been suppressed until the CF sheets break.

In the seismic retrofitting method by winding CF sheets, it is important to design the number and range of layers of CF sheets that are optimal for the dimensions and cross section of the circular steel pier. The cyclic elasto-plastic behavior of circular steel piers is required to accurately predict the deterioration behavior of the envelope of the hysteresis curve and the local deformation mode due to repeated deformation. Investigations mainly by nonlinear analysis methods using three-surface models[8)] have been conducted, and it has been reported that cyclic behavior can be reproduced.

On the other hand, there are few examples of analytical studies on seismic retrofitting of circular steel piers by winding CF sheets, and sufficient studies including modeling have not been conducted. In particular, for the purpose of emergency recovery of a buckled circular steel bridge pier, it is necessary to create a model that is as simple and rational as possible.

Therefore, in this study, in order to quantitatively evaluate the performance recovery by reinforcing and repairing the CF sheet wound in the circumferential direction, an analytical study was conducted and compared with the experimental study of the previous research.

2. OUTLINE OF EXPERIMENT

(1) Test specimen

The specimen used in the experiment of the previous study had a hollow circular cross section with a height of 1900 mm and an outer diameter of 457.2 mm as shown in **Fig. 1**. Stiffening ribs (12 pieces) with a thickness of 16 mm is welded at a position 150 mm from the base of the specimen to prevent the occurrence of buckling near the base. A section change from t_2 = 12.7 mm to t_1 = 9.5 mm is introduced at a position 300 mm from the base so that the buckling does not occur near the stiffener. The specimen was welded to a steel plate with a thickness of 32 mm at the top and bottom to join the bottom plate and the loading block jig. Specimen diameter-thickness ratio parameter R_t and the slenderness ratio parameter λ were designed to be within the applicable range stated in the Road Bridge Specification[9)] as shown in Eqs. (1) and (2).

$$R_t = \frac{R}{t}\frac{\sigma_y}{E}\sqrt{3(1-\nu^2)}, \quad (0.03 \le R_t \le 0.08) \qquad (1)$$

$$\lambda = \frac{2h}{\pi r}\sqrt{\frac{\sigma_y}{E}}, \quad (0.2 \le R_t \le 0.4) \qquad (2)$$

Here, R_t: radius thickness parameter, t: plate thickness, σ_y: yield stress, E_s: Young's modulus of steel, ν: Poisson's ratio of steel, h: effective buckling length, r: secondary radius of the cross section. The yield stress (σ_y), Young's modulus (E_s), and Poisson's ratio (ν) of the steel were determined from the material test. The properties of the pier specimen are summarized in **Table 1**. The axial force ratio, ratio between the weight of the superstructure to the yield load of the pier, used is 0.1 with reference to previous studies[4)].

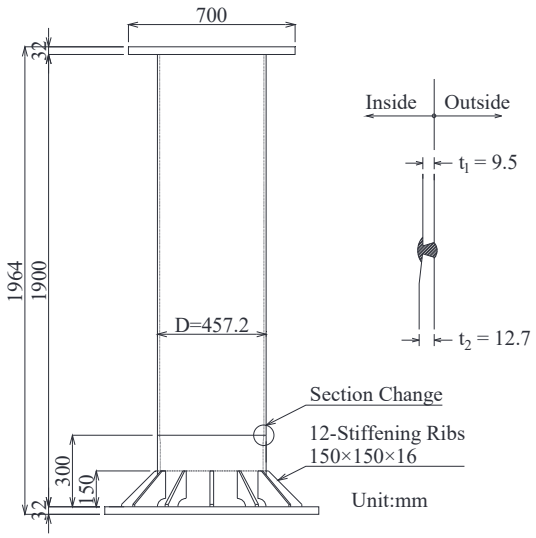

Fig.1 Schematic view of the test specimen.

(2) Loading configuration

The outline of the experimental setup is shown in **Fig. 2**. After applying a constant vertical load (P), to assume the superstructure weight, a horizontal load is applied by displacement control method. The loading position of horizontal load is at the center of the loading block installed at the top of the specimen. As shown in **Fig. 2**, this height is 1832 mm from the top of the stiffeners.

The vertical load (P) was controlled to be constant by load control assuming 10% (492.9 kN) of the yielding axial force as described above. The cyclic loading applied is an increasing multiple of the yield horizontal displacement of the column. The yield horizontal displacement δ_y was investigated using beam theory and FE analysis. The yield horizontal displacement calculated by beam theory was 9.5 mm and the yield horizontal displacement based on FE analysis was 11.6 mm. For the experiment, the yield horizontal displacement δ_y was set to 10 mm.

The direction pulling the horizontal jack is the positive side (+) and the direction pushing is the negative side (-) as shown in **Fig. 2**.

Three circular steel specimens were investigated using this loading setup: unreinforced, reinforced and repair specimen. The unreinforced specimen serves as the control setup while the reinforced and repair specimens are the ones subjected to CF sheet winding method.

(3) Reinforcement by CF sheet wrapping

High strength CF sheets (fiber weight: 300 g/mm^2, tensile strength: 3.4 kN/mm^2, elastic modulus: 245 kN/mm^2) were used for the reinforcement of the circular steel specimen. Seven layers of carbon fiber sheets, with a range of 300 mm, were wound in the circumferential direction at a height of 300 mm to 600 mm from the base. **Fig. 3 (a)** shows the loading program for both the unreinforced and reinforced specimen. In the reinforcement experiment, the carbon fiber sheets were bonded before the increasing cyclic loading was applied.

(4) Repair of buckled specimen by CF sheet wrapping

The loading program for the repair experiment is shown in **Fig. 3 (b)**. For the repair experiment, the specimen was first damaged by the primary loading by increasing cyclic loading. The predetermined damage was defined as the point where the horizontal strength of the circular steel piers dropped to 95% of its peak, and buckling can be visually confirmed[7]. Based on the unreinforced specimen, this damage occurred at the end of ± 6 δ_y loading. After the primary loading (± 6 δ_y) for the repair experiment, the horizontal force of the horizontal jack was released while the vertical load (P). Then, it was repaired by wrapping with 7 layers of CF sheet, and the secondary loading is applied. The secondary loading follows the loading plan used for the unreinforced and reinforced specimen.

3. ANALYTICAL MODEL

(1) Finite element model

Table 1 Specimen Specifications.

Steel grade	STK400
Column Height H (mm)	1900
Outer Diameter D (mm)	457.2
Inner Diameter d (mm)	438.2
Yield Stress σ_y (N/mm^2)	368.9
Young's Modulus E (kN/mm^2)	200
Yield Strain ε_y	1800
Poisson's ratio ν	0.3
Diameter-thickness Parameter R_t	0.074
Slenderness Ratio Parameter λ	0.328
Axial force ratio P/P_y	0.1
Diameter/thickness ratio D/t	48.1

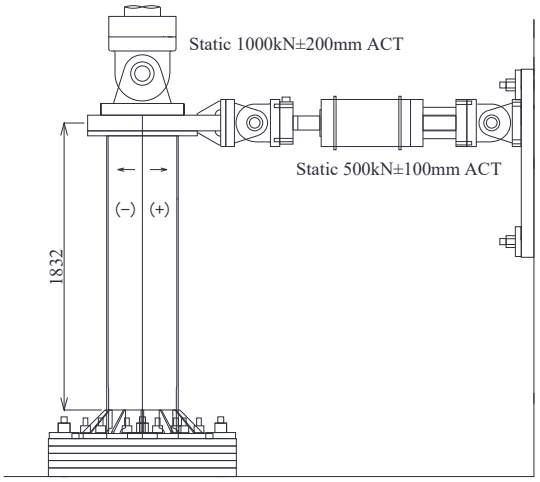

Fig. 2 Outline of Loading Equipment

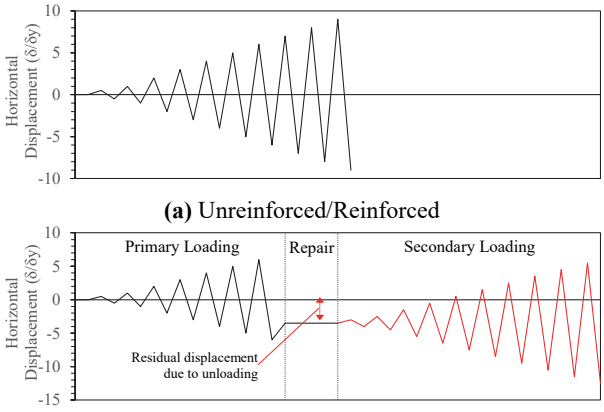

(a) Unreinforced/Reinforced

(b) Repair

Fig. 3 Loading Program

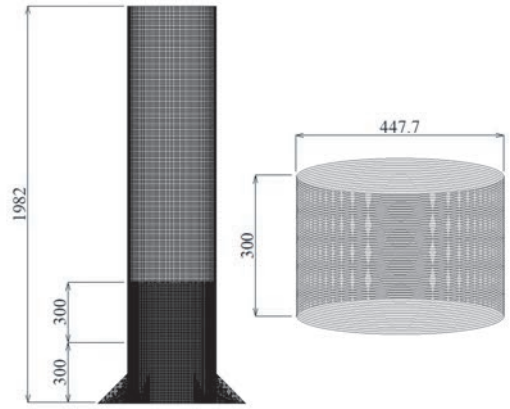

(a) Column **(b)** CF Sheet

Fig.4 Finite Element Analysis Model

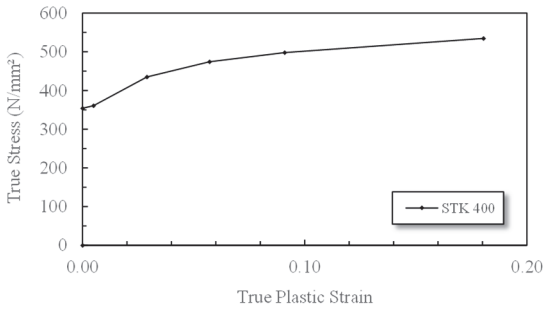

(a) Steel member

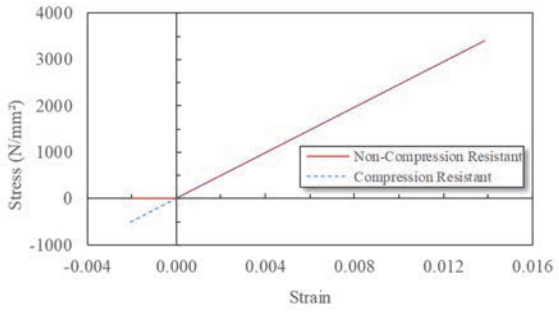

(b) CF sheet

Fig.5 Stress-Strain Relationship

Table 2 Material Properties of Carbon Fiber SheetsType of CF sheet	High strength
CF sheet design thickness t_{cf} (mm)	0.167
Tensile Strength (kN/mm^2)	3.4
Young's Modulus (N/mm^2)	245
Breaking Strain ($\times 10^{-6}$)	14,000

Table 3 Analysis Parameters

Model	Classification	F	P	I
N-F0	Unreinforced	×	-	-
N-F1	Unreinforced	○	-	-
R-F0P0	Reinforced	×	×	-
R-F0P1	Reinforced	×	○	-
S-F0P0I0	Repair	×	×	×
S-F0P0I1	Repair	×	×	○

where F – Vertical Control, P – Compression Resistance, I – Stress Initialization

The finite element analysis of the elasto-plastic behavior due to cyclic loading is performed using the large strain nonlinear procedure of the general-purpose finite element program MSC Marc 2019. The steel specimen was modeled using 4-node thick shell elements with a mesh size of 10 mm x 10 mm. The base of the column up to 600 mm height was modeled using a finer mesh of 5 mm x 5 mm since the buckling occurs within this region[7]. The stiffeners were also modeled using the thick shell elements in MSC Marc. The finite element model of the column specimen is shown in **Fig. 4 (a)**.

The plasticity of steel (up to 18% of plastic strain) was obtained from the results of tensile tests on coupon specimens cut from test specimens as shown in **Fig. 5 (a)**. The true stress – true plastic strain plot from the tensile test was applied in the model together with the kinematic hardening as the constitutive law. The use of kinematic hardening model can provide a relatively close deformation pattern of circular steel piers subjected to cyclic loading[8].

For the boundary conditions, the displacements of all the nodes at the base of the specimen were restrained. A vertical load of 492 kN (10 % of the yielding axial force) is applied at a node located at the top of the column model. The cyclic loading is also applied at the same node using the loading condition shown in **Fig. 3**.

The CF sheets in the finite element analysis were modeled using 2-node truss elements as shown in **Fig. 4 (b)**. The nodes of the truss element of the carbon fiber sheet coincides with the nodes of the shell element of the circular steel pier for continuity. The corresponding area the truss elements are calculated based on the number of layers (n), thickness of CF sheets (t_{cf}) and the effective width (B) as shown in Eq. (3).

$$A_{cf} = B \times t_{cf} \times n \tag{3}$$

Here, number of CF sheets is 7 while the effective width (B) is 5 mm for the middle truss elements 2.5 mm for the truss elements at the top and the bottom.

The resin used for winding the carbon fiber sheet is an important material since it is bonded and integrated with the steel member. However, most of the mechanical contribution is made by the carbon fiber sheet. Thus, to maintain the simplicity of the modeling, only the properties of carbon fiber sheet were used and the properties of the resin were disregarded.

Table 2 shows the material properties of the CF sheet used for the finite element analysis. The Young's modulus of the CF sheet is the average value, and the tensile strength is the characteristic value provided by the manufacturer. The breaking

strain is calculated from the relationship between tensile strength and Young's modulus, assuming linear behavior up to tensile strength. The stress and strain relationship of the CF sheet is shown in **Fig. 5 (b)**. Two stress and strain relationship for the CF sheet was considered for the analysis: compression resistant and non-compression resistant.

The finite element models and analysis parameters considered for this study are summarized in **Table 3** and are discussed in the following sections. In this study, the unreinforced, reinforced, and repair models are denoted as N, R, and S, respectively.

(2) Modeling of vertical loading jack

The unreinforced specimen model was created based on the properties in the previous section. In this model, the modeling of the vertical actuator was examined. The vertical point load applied at the top of the analytical model represents the superstructure weight. In the experiment, the vertical loading jack acts as a swivel attached to the loading frame and to the loading block at the top of the specimen. Strictly speaking, the vertical load does not act vertically at the top of the specimen at all times. On the other hand, in the analysis, it is controlled so that it is always loaded vertically. Two unreinforced model was used for this analysis: vertical jack modeling as vertical point load (N-F0) and vertical jack modeling using a 2-node truss element (N-F1).

Fig. 6 (a) shows the FE analysis model considering the vertical jack (N-F1). The 2778 mm vertical load jack in the experiment was modeled using a two-node truss element connected to the top of the column specimen. As shown in **Fig. 6 (b)**, a pin connection at the top of the two-node truss element is used to represent the swivel motion of the vertical load jack. Initially, a linear expansion coefficient was set for the truss element, then a change in temperature is applied in the element to introduce a constant axial force of 492.9 kN regardless of the position of the vertical jack. The amount of temperature change was controlled appropriately according to the horizontal displacement to keep the axial force constant.

Fig. 7 shows the results of the experiment, the model not controlling the vertical load direction (N-F0) and the model controlling the vertical load direction using thermal stress (N-F1). The relationship between load and horizontal displacement is shown. Comparing the hysteresis curves of the two analytical model, it can be seen that there is a minimal difference between the analytical results. **Table 4** shows the comparison between the maximum loads in the positive and negative direction and the horizontal displacement where it occurred. For the positive direction, the N-F0 model provides a more accurate result while for the negative direction, the N-F1 model governs. However, the difference in the maximum values are small and it can considered that the modeling of the vertical jack has a minimal effect on the analytical results.

From the above results, it is considered that the difference in modeling of the vertical loading jack direction has little effect on the analysis results. Therefore, it was decided to adopt a model with a fixed vertical direction (N-F0) that can be easily evaluated.

(3) CF sheet modeling using truss elements

In the finite element model, the CF sheets are modeled as truss elements as discussed previously. To further assess the validity of using truss elements to represent CF sheet in the finite element model, two parameters were examined: the compression resistance of CF sheet and the initial stresses during activation in the repair model.

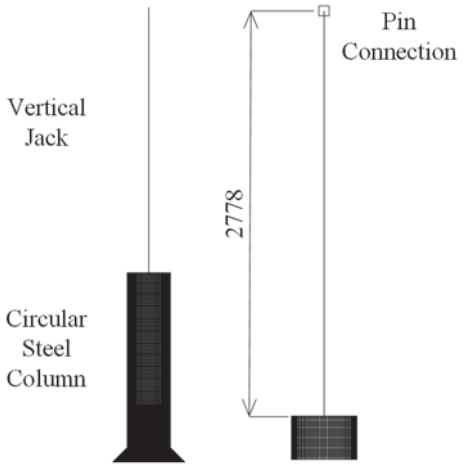

(a) N-F1 Model **(b)** Jack Dimension

Fig.6 Finite Element Analysis Model

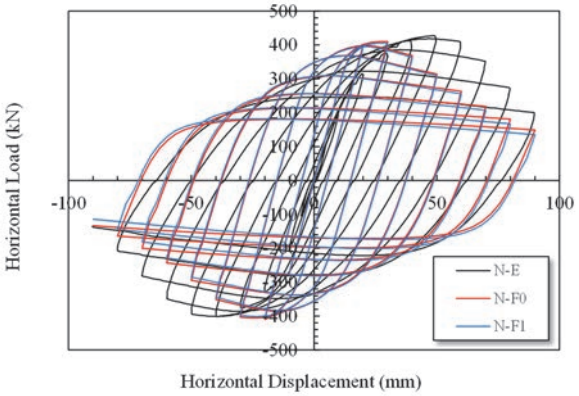

Fig.7 Influence of Vertical Loading Jack on Cyclic Loding

Table 4 Comparison of Maximum Horizontal Loads

Model	(+) Direction	(-) Direction
N-E	411.0 kN (+5δ_y)	392.7 kN (-5δ_y)
N-F0	409.8 kN (+3δ_y)	410.1 kN (-2δ_y)
N-F1	404.9 kN (+3δ_y)	406.5 kN (-2δ_y)

a) Compression resistance of CF sheet

The CF sheet can resist compressive force assuming that the resin has fully impregnated the CF sheet and hardened. However, it must be considered that the carbon fiber sheet cannot fully resist compressive forces when delamination occurs. In the reinforcement experiment, no delamination occurred and only cracking in the circumferential direction was observed. It is possible that the CF sheet in the experiment have resisted the compressive forces during loading. In order to confirm this effect, two models with varying 2-node truss element properties were prepared and compared: a reinforcement model (R-F0P0) that does not resist compressive forces and a reinforcement model (R-F0P1) that resists compressive forces.

The summary of the maximum horizontal loads for each model is shown in **Table 5**. The maximum horizontal load of R-F0P0 was 445.2 kN (+ 3 δ_y) on the positive side, 443.9 kN (-3 δ_y) on the negative side, with an error was 3.8% on the positive side and 0.5% on the negative side. The maximum load of R-F0P1 is + 455.9 kN (+ 4 δ_y) on the positive side, -454.5 kN (-3 δ_y) on the negative side, with an error of 1.5% on the positive side, and 1.9% on the negative side. The maximum horizontal loads are close to the experimental value. Similar with the reinforced model, the horizontal displacement at maximum load is different for the experiment and the analytical results. A decrease in the horizontal capacity can be observed in the analytical models beyond 4 δ_y displacement whereas the experimental results reached the peak at 7 δ_y displacement.

In the experiment, no buckling occurred in reinforced specimen the until the 9 δ_y loading. At the end of the loading, a diamond buckling with an inward buckling at a height of 400 mm at the compression side (-) of the steel column and an outward bulge was observed on the tension side (+) was observed[7]. For the R-F0P0 model, the mode of failure is also by diamond buckling with an inward bulge at both sides was observed at the end of loading. The R-F0P1 model showed a more similar behavior with the experiment at the end of loading. However, for the R-F0P1, the buckling occurred at -5 δ_y displacement which resulted to excessive deformations observed at the end of loading.

Fig. 8 shows the envelope of the hysteresis curve for both directions of the experiment and analysis. The performance recovery of the column specimen was determined by comparing the area under the envelope curve until the final loading. Due to the difference in the behavior from the elastic portion until peak, a huge difference between the absorption capacity was calculated for the experiment and analysis. **Table 6** shows a comparison of energy absorption rates. When comparing the energy absorption of the two reinforcement analytical models with that of the experiment, a difference of about 15% can be seen for R-F0P0, while there's an error of about 7% for R-F0P1.

From these results, the R-F0P1 model may be able to provide a closer approximation of the maximum

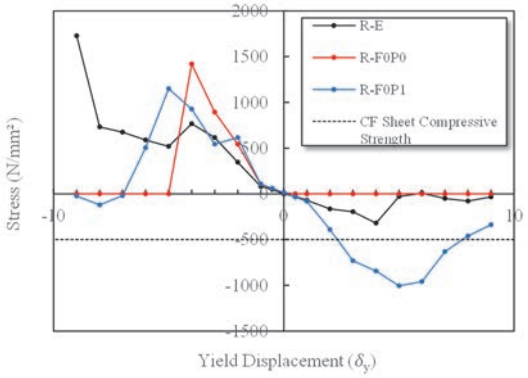

(a) Circumferential Stress at Pt. 1

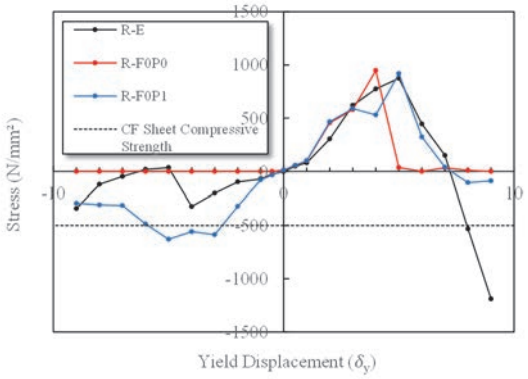

(b) Circumferential Stress at Pt. 2

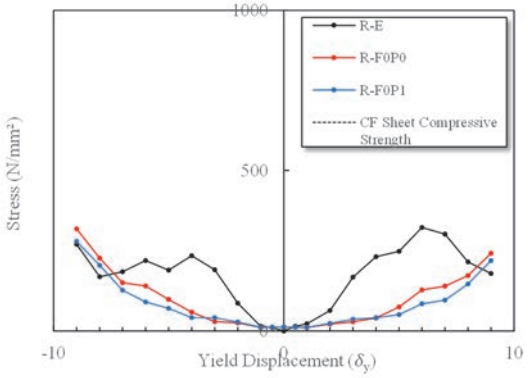

(c) Circumferential Stress at Pt. 3

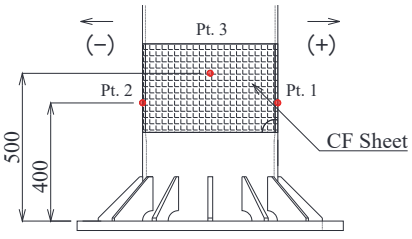

(d) Stress Measurement Location

Fig.9 Circumferential Stress of CF Sheet

load and energy absorption capacity. On the other hand, the circumferential stress of the CF sheet in the experiment and analysis model shown in **Fig. 9** shows that the circumferential stress generated in the carbon fiber sheet during the experiment was very small. However, in the case of R-F0P1, compressive strain exceeding the compressive strength of general carbon fiber sheet of 500 N/mm^2 was generated, indicating that the reinforcing effect of carbon fiber sheet was overestimated. From the results, R-F0P0, which is conservative, is adopted in modeling a reinforcing sheet using two-node truss elements. When considering the pressure resistance of carbon fiber sheet, it is necessary to appropriately consider the material strength.

b) Initial stress in the CF sheet upon activation

In the repair experiment, CF sheet is bonded to the column after it reached the ultimate limit (6 δ_y) in the primary loading. The CF sheet is manually bonded to the buckled circular steel pier, so when the resin of the CF sheet is cured, the CF sheet is stress free. In the analysis of the repair specimen, if special control is not performed when activating the two-node truss element, the carbon fiber sheet elements exhibits a different initial condition from the actual repair procedure. Therefore, in order to confirm the influence of the initial stress in the CF sheet elements, a model that controls the stress initialization upon activation (S-F0P0I1) and a model that uses the default settings in the activation (S-F0P010) were created and compared using a pushover analysis. For simplicity, only a static loading with a maximum displacement of 9 δ_y was applied to check the stress initialization. The CF sheet elements are deactivated until ultimate limit is reached (+6 δ_y) and are activated beyond this point.

Fig. 10 shows the plot of the circumferential stress of the CF sheet in the compression side of the column after activation of the truss elements, right after activation and at the final loading of the models. Here, we can see that upon activation, there are no stresses in the S-F0P0I1 model while in the S-F0P0I0 model there is an initial stress distribution with a maximum of 510 N/mm^2. This initial stress can be attributed to the buckling of the column due to the static loading. In the increment right after activation, a maximum difference of 484 N/mm^2 between the two models can be observed in the buckling location. In the final loading, the stress difference at all points are almost negligible except for the peak of the buckling region (h = 370 to 380 mm) with a difference of 340 N/mm^2. From this graph, it can be seen that the initial stress has a huge impact upon activation, but the difference decreases eventually after several loading. In addition, the CF sheet elements here were modeled not to resist compressive forces resulting to zero stresses at certain heights.

Comparing the load and displacement curve of the pushover analysis, it can be seen that both models exhibited the same behavior as shown in **Fig. 11**. The maximum loading for each model after the repair using CF sheet elements are 422.8 kN for the S-F0P0I0

Table 5 Comparison of Maximum Horizontal Loads

Model	(+) Direction	(-) Direction
R-E	459.5 kN (+7 δy)	441.9 kN (-6 δy)
R-F0P0	445.2 kN (+3 δy)	443.9 kN (-3 δy)
R-F0P1	455.9 kN (+4 δy)	454.4 kN (-3 δy)

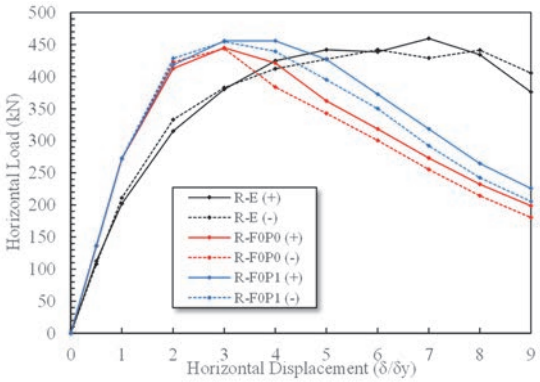

Fig.8 Load-Displacement Envelope Curve of Reinforced Specimen

Table 6 Comparison of Energy Absorption Rate

Model	(+) Direction	(-) Direction
R-E	1.000	1.000
R-F0P0	0.862	0.830
R-F0P1	0.942	0.907

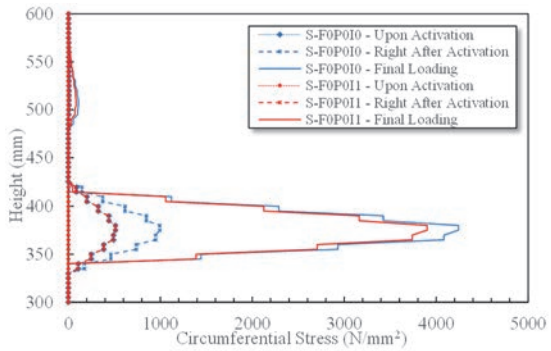

Fig.10 Circumferential Stress Distribution in the Compression Side of the Pushover Analysis

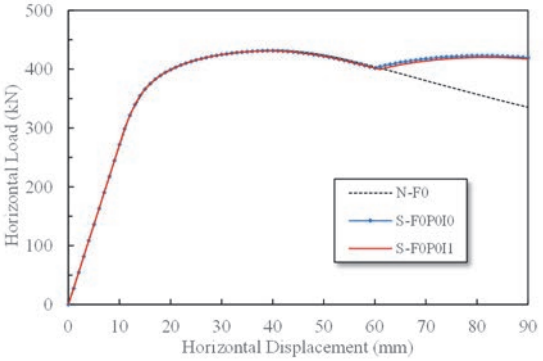

Fig.11 Load and Displacement Curve of the Pushover Analysis

model and 420.1 kN for the S-F0P0I1 model. From these results, it can be confirmed that even though there are differences in the CF sheet stresses due to the stress initialization parameter, it has no significant effect on the loading capacity. Thus, to maintain the simplicity of the modeling, the S-F0P0I0 governed and the default activation settings was used for the repair model.

4. COMPARISON OF EXPERIMENTAL AND ANALYTICAL MODEL

(1) Buckling mode comparison

In this section, the modes of buckling of the test specimens in the experiment and in the analytical model are compared. In **Fig. 12**, the buckling mode at the end of loading for the experimental and analytical model of the unreinforced specimen are shown. It can be seen that the N-F0 model was able to reproduce the elephant foot buckling that occurred in the experiment. The location of buckling for the analytical model occurred at a height of 400 mm in the direction of the loading and 375 mm at the axis perpendicular to the loading. In the experiment, the buckling occurred at 400 mm and 350 mm for the axis parallel and perpendicular to loading, respectively.

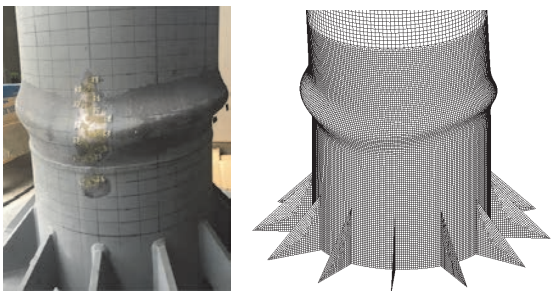

(a) Experiment **(b)** FEM

Fig.12 Comparison of Failure Mode in Unreinforced Specimen

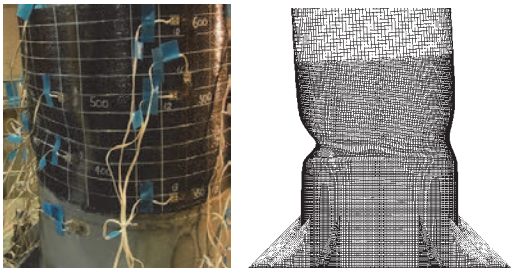

(a) Experiment **(b)** FEM

Fig.13 Comparison of Failure Mode in Reinforced Specimen

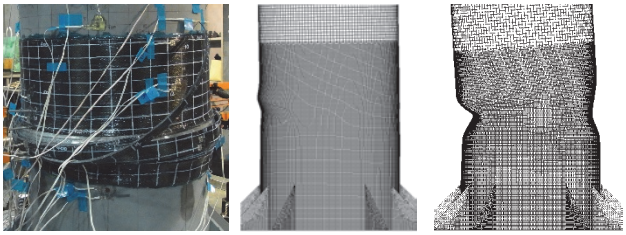

(a) Experiment **(b)** FEM (Primary) **(c)** FEM (Secondary)

Fig.14 Comparison of Failure Mode in Repair Specimen

In the reinforcement experiment by CF sheet wrapping, no sign of buckling was observed until the 9 δ_y loading. An inward buckling at a height 400 mm from the based was observe at the completion of loading as shown in **Fig. 13 (a)**. In the analytical model (R-F0P0), deformation initially occurred at -4 δ_y loading where the tension side buckled inward at height of 360 mm. At the end of loading, both sides of the column have deformed inside for about 30 mm at the same height as shown in **Fig. 13 (b)**.

In the repair experiment, the primary loading was performed up to +6 δ_y before the repair, and as a result, the bulge was formed at a position of 400 mm from the base. However, at +8 δ_y of the secondary loading, almost all of the CF sheet in the range of 375 to 450 mm from the base was broken[7]. **Fig. 14 (a)** shows the state of the repaired column at the end the loading.

Due to the difference in the horizontal displacement at maximum loading observed in the unreinforced specimen, it was decided to change the loading condition for the S-F0P0I0 model. From the unreinforced model (N-F0), it was observed the the ultimate limit occurred at 4 δ_y. Hence, in order to compare the repair behavior at the same condition, the primary loading applied for the repair specimen is only until 4 δ_y then secondary loading, same as in the experiment, was applied after. **Fig. 14 (b)** and **Fig. 14 (c)** shows the mode of buckling in the S-F0P0I0 model. After the primary loading, an outward buckling was observed which is similar to that of in the experiment.

In the analytical model, after applying the CF sheet elements, the outward bulge due to the primary loading was suppressed which was not the same for the experiment. As seen in **Fig. 14 (a)**, the CF sheet cracked in the circumferential direction and have peeled from the column. The debonding of CF sheet and the failure of resin was not considered in the FEM model which resulted to a very different buckling deformation. In addition, as the horizontal displacement applied increases, the steel column tends to buckle inside because of the circumferential constraint added by the rigidity of the CF sheet elements.

(2) Horizontal load and horizontal displacement relationship

The relationship between the horizontal load and displacement for the unreinforced model is shown in **Fig. 7**. Based on this graph, a huge difference has already been observed between the experimental and analytical model. Although the analytical results were able to provide a close approximation of the maximum horizontal load, it was not able to match

the horizontal displacement in which the maximum load occur. The maximum load was reached earlier at +3 δ_y as compared to the +5 δ_y observed in the experiment. This resulted to a much lower capacity at larger displacements for the analytical model.

For the reinforced model, shown in **Fig. 15 (a)**, the maximum loading was reached at different displacement just like the unreinforced model. In the analysis, the maximum horizontal force was reached after 3 δ_y loading which is not the same as the experiment where the maximum load occurred after 7 δ_y loading. The reinforced model (R-F0P0) was not able to reproduce the hysteretic behavior experiment but it was able to provide the loading capacity of the specimen. The maximum loads in the positive and negative direction are shown in Table 6. It can be seen here that the maximum horizontal loads are almost the same with just an error of 3% in the positive direction and 0.5% in the negative direction.

The results of the secondary loading on the repair specimen are shown in **Fig. 15 (b)**. In this plot, it can be seen that the horizontal displacement during the maximum loading was also different just like in the other specimen. In the experiment, the maximum horizontal load of 411.1 kN is much higher than the 377.1 kN obtained in the analytical model with an error of 8%. The same case was observed in the negative direction with the experimental value of 378 kN much higher than the 359.7 kN obtained in the analytical model with an error of 5%. This can be attributed to the different buckling mode that in the experiment and analytical model. The analytical model experienced a much severe buckling resulting to a lower capacity.

(3) Comparison of performance recovery by energy absorption

Fig. 16 shows the envelope curve of the experimental and analytical results for all specimen. The envelope curve was obtained from the relationship between the horizontal load and the horizontal displacement. The vertical axis is the ratio between the horizontal load and yield horizontal load (H_y) while the horizontal axis is the ratio between the horizontal displacement and the yield horizontal displacement (δ_y). **Tables 6** and **7** show the comparison of maximum horizontal loads and the comparison of energy absorption rate, respectively.

The energy absorption of the specimen is evaluated by calculating the area under the envelope curves. Since the envelope curves of the analytical result does not have the same behavior as the experiment, the energy absorption rates were calculated separately for the experimental and analytical data.

Table 6 Comparison of Maximum Horizontal Loads

Classification		Experiment	Analysis
R	+	459.5 kN	445.2 kN
	-	441.9 kN	443.9 kN
S	+	411.1 kN	377.1 kN
	-	378.0 kN	359.7 kN

Table 7 Comparison of Energy Absorption Rate

Classification		Experiment	Analysis
N	+	1.000	1.000
	-	1.000	1.000
R	+	1.169	1.136
	-	1.266	1.133
S	+	0.957	1.018
	-	0.904	0.984

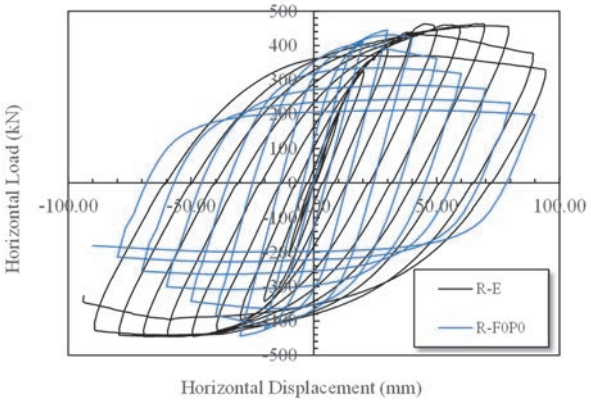

(a) Reinforced Specimen

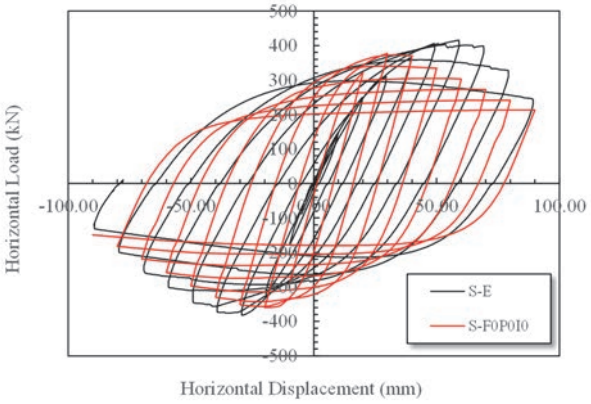

(b) Repair Specimen

Fig.15 Load and Displacement Relationship

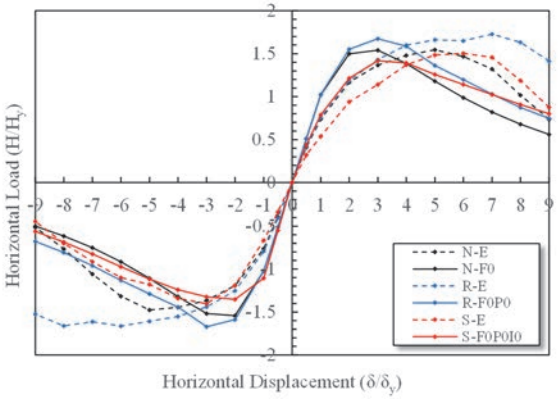

Fig.16 Summary of the Envelope Curve

The energy absorption rate for the reinforced and repaired specimen are calculated as a ratio with the energy absorption of the unreinforced model.

In the analytical results, the energy absorption for the reinforced model (R-F0P0) is higher than the unreinforced model by about 13% in both positive and negative directions. However, in the experiment, the reinforced specimen increased the energy absorption by 17% in the positive direction and 27% in the negative direction.

In the repair model, the S-F0P0I0 have provided higher absorption rates compared to the experiment. A difference of about 5% in the positive direction and 10% in the direction was observed. Higher values were observed since the peeling and cracking of the CF sheet was not considered in the analytical model.

From these results, it is clear that the maximum load can be predicted to some extent by the analysis method using a simple model, but it is difficult to evaluate the energy absorption rate. In order to accurately understand the elasto-plastic behavior of the carbon fiber sheet wrapping reinforcement, it is necessary to model the compression properties and fracture behavior of the carbon fiber sheet more accurately in the range where large horizontal displacement is applied.

5. CONCLUSIONS

In this study, regarding the reinforcement and repair of circular steel piers by carbon fiber sheet wrapping conducted in a previous study, the modeling of carbon fiber sheets and nonlinear analysis considering buckling deformations was performed and studied. The results obtained are shown below.

(1) In considering the direction of the vertical jack actuator, which represents the superstructure weight, the difference in the experimental and analytical models are negligible and has a minimal effect on the analysis result.

(2) It was found that it was possible to evaluate the maximum load in the analysis model of the carbon fiber sheet wrapping reinforcement of the circular steel pier using the two-node non-restraining truss element. However, the behavior and energy absorption after the maximum horizontal force showed a large difference between the experiment and the analysis because the modeling of carbon fiber sheet failure was not enough.

(3) In the analysis of CF sheet repair of a buckled circular steel pier, the effect of the initial stress distribution upon activation has a minimal effect on the final state of the model. Therefore, the initialization of stress when the two-node truss element is activated can be neglected for simpler modeling.

(4) The finite element modeling using the kinematic hardening constitutive model and the plasticity behavior obtained from tensile tests can provide the loading capacity for all specimens which are in agreement with the experiment. However, the modeling used does not provide an accurate representation of the load and displacement relationship observed in the experiments of the previous study.

As a future work, detailed modeling to improve the unreinforced specimen must be focused on. In particular, modifications in the model must be done to provide load and displacement relationships similar to that of the experiment. The influence of modeling the CF sheets using 2-node truss elements in the performance recovery can be further verified if the load and displacements match the experimental results. In addition, the peeling of the carbon fiber sheet and the behavior when the carbon fiber sheet reaches the breaking strain must also be integrated in the model to improve the results in the repair model.

REFERENCES

1) Hanshin Expressway Management Technology Center: Overcoming the Great East Japan Earthquake, Recovery Construction Magazine, Hanshin Expressway Public Corporation, 1997.
2) Concrete Engineering Committee of the Japan Society of Civil Engineers: Guidelines for repair and reinforcement of concrete structures using continuous fiber sheets, Concrete Library 101, 2000.
3) (Foundation) Public Works Research Center: Retrofit guidelines of the steel piers by carbon fiber sheet (draft), 2002.7
4) Watanabe, T., Ishida, K., Hayashi, K., Yamaguchi, T., Ikeda, N.: Seismic reinforcement of steel bridge piers using a carbon fiber sheet, *Journal of Structural Engineering*, Vol.48A, pp. 725-734, 2002.3
5) Matsumura, M., Kitada, T., Tokubayashi, M., Ikeda, K., Okada, T.: Experimental study on seismic retrofitting of steel pier columns with carbon fiber sheets attached circumferentially, *Proceedings of the Japan Society of Civil Engineers*, No.766/ I-68, pp. 17-31, 2004.7
6) Komuro, M., Kishi, T., Mikami, H., Nishi, H.: AFRP sheet wrapped around the static loading tests on seismic reinforcement of the real scale steel pipe piers by, *Journal of Structural Engineering*, Vol.52A, pp. 1327-1336, 2006.3
7) Okazaki, N., Nakamura, K., Kishi, K., Matsui, T., Setouchi, H.: Study on performance recovery of buckling damaged circular steel piers by rolling up carbon fiber sheet, *Journal of Japan Society of Civil Engineers A1 (Structure and Earthquake Engineering)*, Vol.73, No.1, pp. 69-83, 2017.5
8) Goto, Y., Wang, K., Takahashi, N., Obata, M.: Analysis of steel piers under cyclic loading by finite element method and material constitutive law, *Journal of Japan Society of Civil Engineers*, No.591, I-43, pp. 189-206, 1998.
9) Japan Road Association: Specifications for Road Bridges, Commentary, (1) Seismic Design, pp. 225-230, 2012.

(Received August 28, 2020)